
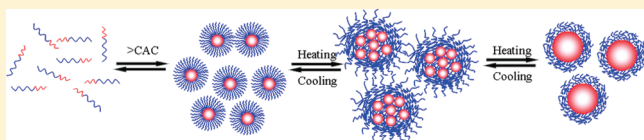


# Thermosensitive Behavior of Poly(ethylene Glycol)-Based Block Copolymer (PEG-*b*-PADMO) Controlled via Self-Assembled Microstructure

Qianling Cui,<sup>†,‡</sup> Feipeng Wu,<sup>\*,†</sup> and Erjian Wang<sup>†</sup><sup>†</sup>Technical Institute of Physics and Chemistry, Chinese Academy of Sciences, Beijing 100190, P. R. China<sup>‡</sup>Graduate University of Chinese Academy of Sciences, Beijing 100049, P. R. China Supporting Information

**ABSTRACT:** Stimuli-responsive, well-defined diblock copolymers (PEG-*b*-PADMO) comprising poly(ethylene glycol) (PEG, DP (degree of polymerization) = 45) as the hydrophilic and temperature-sensitive part and poly(*N*-acryloyl-2,2-dimethyl-1,3-oxazolidine) (PADMO, DP = 18–47) as the hydrophobic and acid-labile part self-assembled in water into spherical micelles with high aggregation number. The micellar structures and thermally induced phase transitions of the copolymers were investigated with <sup>1</sup>H NMR spectroscopy, light scattering, microscopy, turbidimetry, and fluorescence techniques. Thermoresponsive phase transitions of the copolymers in water were controlled via formation of core–shell-type micelles with densely compact PEG corona. Their lower critical solution temperatures (LCSTs) were modulated within the range 40–72 °C by varying PADMO block length. This unusually low LCST was attributed to the densely packed PEG structure in the polymer micelles, which resulted in strong n-clustering attractive interactions and insufficient hydration of PEG chains in the shell and greatly enhanced the thermosensitivity. The LCST behavior can also be modulated by partial acid hydrolysis of PADMO segments through the resulting change of hydrophobicity.



## 1. INTRODUCTION

Over the past decades, thermoresponsive polymers have received a great deal of attention for nanotechnology and biotechnology applications such as smart gels, sensors, drug-delivery vehicles, and tissue engineering.<sup>1,2</sup> These polymers usually dissolve when cooled and separate from the aqueous solution when heated above the phase transition temperature (lower critical solution temperature; LCST). Hence, temperature can be used as a simple external trigger for controlling the hydrophobicity and therefore the structures and shapes of these macromolecules. The most extensively investigated thermoresponsive polymer is poly(*N*-isopropylacrylamide) (PNIPAM), which undergoes a sharp coil-to-globule transition in water around 32 °C, changing from a hydrophilic state below this temperature to a hydrophobic state above it. PNIPAM is commonly considered to be as the “gold standard”. However, despite its widespread popularity in material science, PNIPAM has disadvantages such as hysteresis in the heating–cooling cycle<sup>3</sup> and significant influence of the molecular weight and end groups for short chain polymers.<sup>4</sup> Moreover, the formation of hydrogen bonded complexes between PNIPAM and proteins complicates its use in biotechnology applications.<sup>5,6</sup>

Poly(ethylene glycol) (PEG), also referred to as poly(ethylene oxide) (PEO), is neutral, water-soluble, biocompatible, nontoxic, nonimmunogenic, and FDA approved and is the most used material in biological and pharmaceutical applications.<sup>7</sup> PEG has both hydrophilic and hydrophobic characteristics because of the

presence of the ether groups, which show affinity for water molecules via hydrogen bonding, as well as the converse behavior of  $-\text{CH}_2\text{CH}_2-$  segments, which repel water. PEG can dissolve in water because water molecules form a layer around the macromolecule. PEG as a hydrophilic building block has been widely used as a constituent of a variety of functional polymers, to enhance the dispersion of hydrophobic block/micelles in aqueous solution. In principle, PEG should possess interesting thermosensitive behavior similar to that of PNIPAM, via dehydration at elevated temperature. However, the LCST of PEG is typically higher than 100 °C and depends on the molecular weight.<sup>8–10</sup> Hence, the main challenge is to tune the phase transition temperature to an appropriate range.

During the past few years, thermoresponsive polymers comprising short chain oligo(ethylene glycol) in side chains have been developed as an alternative to PNIPAM.<sup>11–16</sup> The LCST of these polymers can be adjusted through control of molecular structure and composition of the polymer. Lutz et al.<sup>11,12</sup> prepared well-defined thermoresponsive copolymers of poly(2-(2-methoxyethoxy)ethyl methacrylate-*co*-oligo(ethylene glycol) methacrylate) (P(MEO<sub>2</sub>MA-*co*-OEGMA)). Compared with PNIPAM, this type of copolymer exhibited only slight hysteresis, and the thermoresponsiveness was only slightly influenced by the

Received: January 21, 2011

Revised: April 13, 2011

Published: April 27, 2011

degree of polymerization (DP), ionic strength, and concentration. The LCST could be varied from 25 to 90 °C, depending on the number of ethylene glycol side-chain units (or the molar fraction of the monomer). Similar results were reported by several research groups by varying the copolymer composition or oligo(ethylene glycol) monomer structure.<sup>13–15</sup> In addition, Hua et al.<sup>16</sup> synthesized a double thermosensitive diblock copolymer comprising poly(methoxytri(ethylene glycol) acrylate) and poly(4-vinylbenzyl methoxytris(oxyethylene) ether) and found multiple phase transitions in aqueous solution with increasing temperature. An important difference between linear PEG and polymers of this type is that the latter have a carbon–carbon nonpolar backbone and multiple short oligo-(polyethylene glycol) side chains.

In recent times, other strategies for preparing thermosensitive polymers with tunable phase transition temperature have been proposed, involving incorporation of a temperature-sensitive polymer,<sup>17–26</sup> such as poly(*N*-substituted acrylamide) on solid substrates or at an interface with a sufficient density, referred to as polymer brush.<sup>17–22</sup> Such a densely compact structure gives rise to strong chain interactions and results in a substantial change of thermally induced phase transition behavior of the polymer chains, which differs markedly from the behavior of conventional thermoresponsive polymer chains in solution. Tenhu and co-workers<sup>17,18</sup> reported that linear PNIPAM homopolymer chains highly grafted to gold nanoparticles exhibited two distinct phase transitions, corresponding to the sequential collapse of inner and outer PNIPAM segments. It was suggested that the PNIPAM segments close to the gold surface were more densely compact and less hydrated and underwent the first transition at lower temperature. Kono et al.<sup>19–21</sup> synthesized dendrimers of poly-(amidoamine) or poly(propylenimine) that were modified at the periphery with isobutylamine (IBAM). Their LCSTs decreased remarkably with increasing dendrimer generation because the density of the terminal IBAM groups concomitantly increased. A similar phenomenon was observed for the hyperbranched polymers modified with temperature-responsive groups at the chain ends, which have been reported by several research groups.<sup>23–26</sup> As an example, hyperbranched poly(glycidol) modified with NIPAM terminal groups exhibited thermally induced phase transitions at significantly lower temperatures than the LCST of PNIPAM, depending on the DP. The reduced LCSTs were attributed to increase of the terminal group density and therefore van der Waals interactions, resulting in a lower cloud point of polymers with higher DP.

In view of the unique characteristics of structures with compact molecular organization as mentioned above, the aim of the present study was to develop a new class of thermoresponsive polymers based on PEG as a temperature-sensitive element capable of forming core–shell type micelles with densely compact PEG corona. Such structures tend to be more easily prepared than thermosensitively modified dendrimer or hyperbranched polymers. Thus, they may be more useful from a practical viewpoint. We expected these designed polymers to exhibit a moderate phase transition temperature far lower than the high value of the PEG homopolymer precursor, by controlling the structure and organization of the polymer chains at the microscopic level.

Recently, we developed a novel stimuli-responsive amphiphilic diblock copolymer (PEG-*b*-PADMO) comprising PEG as the hydrophilic part and poly(*N*-acryloyl-2,2-dimethyl-1,3-oxazolidine) (PADMO) as the acid-labile hydrophobic part, by reversible addition–fragmentation chain transfer (RAFT) polymerization.<sup>27</sup> These

copolymers self-assembled in water to form core–shell type micelles with high aggregation number. In the study of the pH-responsive behavior, we found, unexpectedly, that these copolymers exhibited thermal transitions at elevated temperature but far below the cloud point of 170–180 °C for the PEG ( $M_w = 2.0 \times 10^3$  g mol<sup>−1</sup>) precursor. In the present study, the PEG-*b*-PADMO copolymers were used as a model system for investigation of thermoresponsive behavior in relation to the microstructure of aggregates of the polymers in aqueous solution. The study provided useful information on control of the thermally induced transition in a lower-temperature range, for smart copolymers based on the temperature-sensitive functionality of PEG. Thus, the micellar structure, thermally induced phase transition behavior, and aggregation mechanism were studied in detail by <sup>1</sup>H NMR spectroscopy, static and dynamic light scattering, transmission electron microscopy, turbidimetry, and fluorescence techniques, and a proposed mechanism was discussed.

## 2. EXPERIMENTAL SECTION

**Materials.** *N*-Acryloyl-2,2-dimethyl-1,3-oxazolidine (ADMO) and PEG-CTA were synthesized as previously reported.<sup>27</sup> 2,2'-Azobis(isobutyronitrile) (AIBN) was recrystallized twice from ethanol and stored in the refrigerator. 1,4-Dioxane was distilled over CaH<sub>2</sub> prior to use. Other solvents and reagents were purchased from Beijing Chemical Reagent Company (China) and used as received. All aqueous solutions were prepared using deionized water.

**Synthesis of Poly(ethylene Glycol)-*block*-poly(*N*-acryloyl-2,2-dimethyl-1,3-oxazolidine) (PEG-*b*-PADMO).** A series of PEG-*b*-PADMO copolymers were synthesized via RAFT polymerization using PEG-CTA as a macro-RAFT agent.<sup>27</sup> To obtain diblock copolymers with different PADMO block lengths, the molar ratio of monomer to PEG-CTA was varied at 20, 30, 45, and 50, respectively, while the molar ratio of PEG-CTA to initiator was kept at 10. As an example, for synthesis of copolymer with PADMO length 30 units, 0.70 g of ADMO, 0.37 g of PEG-CTA, and 2.5 mg of AIBN were dissolved in 5 mL of 1,4-dioxane. The solution was deoxygenated by purging with nitrogen gas for 30 min. Polymerization was carried out in a water bath at 70 °C for 24 h and terminated by an ice bath and exposure to air. The polymer was isolated by three precipitation–dissolution steps from tetrahydrofuran (THF) to hexane. After drying under vacuum at room temperature for 24 h, the polymer was obtained as a pink powder. The DP of these copolymers as determined by <sup>1</sup>H NMR was 18, 28, 40, and 47; the corresponding copolymers are denoted E<sub>45</sub>A<sub>18</sub>, E<sub>45</sub>A<sub>28</sub>, E<sub>45</sub>A<sub>40</sub>, and E<sub>45</sub>A<sub>47</sub>, respectively.

**NMR Spectroscopy.** <sup>1</sup>H NMR spectra (400 MHz) were recorded in deuterated solvents at 25 °C with a Bruker DPX-400 NMR spectrometer. Temperature-dependent <sup>1</sup>H NMR spectra of the copolymers in D<sub>2</sub>O at temperatures from 40 to 60 °C were recorded with a Bruker DMX-300 NMR spectrometer.

**Gel Permeation Chromatography (GPC).** The weight average molecular weights ( $M_w$ ) and polydispersity index (PDI,  $M_w/M_n$ ) were estimated by gel permeation chromatography (GPC) on equipment composed of a Waters 1525 binary HPLC pump in conjunction with a Waters 2414 refractive index detector and three Waters Styragel columns. THF was used as the eluent at a flow rate of 1 mL min<sup>−1</sup>, and linear polystyrene standards were used for calibration.

**Transmission Electron Microscopy (TEM).** Transmission electron microscopy was carried out with a JEOL JEM-2100 instrument with accelerating voltage 200 KV. The sample was prepared by placing a drop of the copolymer solution on a carbon-

coated copper grid (400 mesh), staining with 1% (w/v) uranyl acetate solution, and allowing the sample to dry in air. For morphology determination during the LCST transition, the micellar solution was equilibrated for at least 5 h at predetermined temperature, as well as the preparation and evaporation of samples.

**Dynamic Light Scattering (DLS).** Average hydrodynamic radius and distributions of the aggregates formed in aqueous solutions of the polymers were determined using a DynaPro NanoStar instrument (Wyatt Technology), with a He–Ne laser ( $\lambda = 659$  nm) operated at 10 mW. The measurements were made at the scattering angle  $\theta = 90^\circ$  at  $25^\circ\text{C}$ . Prior to measurement the polymer solutions were clarified by filtering through Millipore membranes with  $0.22\ \mu\text{m}$  pore size. The hydrodynamic radius  $R_h$  was calculated using the Stokes–Einstein equation  $R_h = k_B T / 6\pi\eta D$ , where  $D$  is the diffusion coefficient,  $k_B$  the Boltzmann constant,  $T$  absolute temperature, and  $\eta$  the viscosity of the solvent.

**Static Light Scattering (SLS).** Static light scattering (SLS) measurements were carried out with a Wyatt DAWN HELEOS-II Multi-Angle light scattering instrument equipped with a He–Ne laser ( $\lambda = 658$  nm) as the light source. The apparent weight average molecular weight ( $M_{w,\text{app}}$ ) was estimated from the relation<sup>28</sup>

$$\frac{KC_p}{R_\theta} = \frac{1}{M_{w,\text{app}}} \left( 1 + \frac{1}{3} \langle R_g \rangle^2 q^2 \right) + 2A_2 C_p \quad (1)$$

where  $R_\theta$  is the Rayleigh ratio;  $R_g$  is  $z$ -average radius of gyration;  $A_2$  is the second virial coefficient;  $q$  is the magnitude of the scattering vector; and  $K = 4\pi^2 n^2 (dn/dc_p)^2 / N_A \lambda^4$ , with  $dn/dc_p$  being the refractive index increment against polymer concentration ( $C_p$ ) and  $N_A$  being Avogadro's number.  $R_\theta$  was determined by subtracting the solvent scattering from the total scattering of the solution. By measuring  $R_\theta$  for a range of  $C_p$  and  $\theta$ , values of  $M_{w,\text{app}}$ ,  $R_g$ , and  $A_2$  were estimated from Zimm plots. Toluene was used for calibration of the instrument. The refractive index increment  $dn/dc_p$  of the block copolymers was determined with a Wyatt Optilab rEX differential refractometer.

**Preparation of Micellar Solution.** A stock aqueous solution of block copolymer was prepared by dissolving the polymer powder in water followed by overnight refrigeration to ensure complete dissolution, then diluting with deionized water to obtain the desired concentration. Each sample was equilibrated at least for 1 day prior to measurement.

**Determination of Critical Aggregation Concentration (CAC).** Critical aggregation concentration (CAC) values of the copolymers were determined by steady-state fluorescence spectroscopy using pyrene as the probe. A saturated aqueous solution of pyrene with concentration of  $1.0 \times 10^{-6}\ \text{mol L}^{-1}$  was used for preparation of aqueous solutions of the copolymer, whose concentration was varied from  $1.0 \times 10^{-4}$  to  $1.0\ \text{mg mL}^{-1}$ . Excitation spectra of pyrene were obtained with a Hitachi F-4500 fluorescence spectrometer in the range 300–370 nm with emission wavelength 383 nm. The CAC was determined from a plot of the ratio of fluorescence intensity at 338 and 333 nm versus the polymer concentration.

**Phase Transition Measurements by Turbidimetric Method.** The cloud points of the aqueous solutions of the polymers were investigated on a Hitachi U-3900 UV–vis spectrophotometer together with a Brookfield temperature controller. The transmittance of aqueous solutions of polymer at  $\lambda = 600$  nm was recorded in a 1.0 cm path length quartz cell. In the heating–cooling cycle, the rate of heating or cooling was set at  $1^\circ\text{C min}^{-1}$  with hold steps

of 10 min at each temperature. The cloud point was determined from 50% of the transmittance versus temperature plot.

### 3. RESULTS AND DISCUSSION

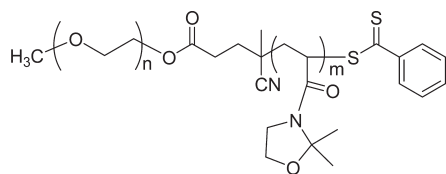
**3.1. Micellar Structure.** The chemical structure of the PEG-*b*-PADMO copolymers is shown in Scheme 1. A series of copolymers with different PADMO block length ( $m = 18$ –47) and fixed PEG block length ( $M_w = 2.0 \times 10^3\ \text{g mol}^{-1}$ ,  $n = 45$ ) were synthesized to vary the size and structure of the micelles formed in water. Relevant experimental data are given in Table 1, where PEG and PADMO segments with given polymerization degree are denoted as  $E_{45}$  and  $A_m$ , respectively.

The PEG-*b*-PADMO copolymers were soluble in water, forming transparent micellar solutions at ambient temperature. These micelles comprised compact hydrophobic cores of PADMO surrounded by water-soluble PEG shells. The core–shell structure of the micelles was supported by  $^1\text{H}$  NMR spectra and TEM images.<sup>27</sup> Figure 1a shows that the characteristic signals of PEG and PADMO (peak a, ascribed to the protons of the dimethyl group) were clear and sharp in  $\text{CDCl}_3$ . While the proton peak of PADMO almost disappeared in water (Figure 1b), the PEG signal remained sharp and intense. This is reflecting the fact that the molecular motion of the PADMO core-forming block in the micelles was strongly restricted, whereas the PEG shell block was in a highly dynamic state. The CAC of the polymer micelle was determined using pyrene as a fluorescent probe from the ratio ( $I_{338}/I_{333}$ ) of excitation intensities at 338 and 333 nm, which reflected the transition of pyrene from a polar environment to an apolar micellar core environment.<sup>29,30</sup> The excitation spectra of pyrene in solutions of  $E_{45}A_{28}$  as an example are shown in Figure 2. As the polymer concentration increased, the peak at 333 nm showed a clear shift to longer wavelength. The value of CAC was estimated from the plot of  $I_{338}/I_{333}$  versus polymer concentration (Figure 2, inset). The CAC values thus determined for PEG-*b*-PADMO copolymers with various compositions are given in Table 1. As expected, the CAC values were strongly dependent on the length of the hydrophobic PADMO block, with the relative order  $E_{45}A_{18} > E_{45}A_{28} > E_{45}A_{40} > E_{45}A_{47}$ .

To further elucidate their nature and structure, the polymer micelles formed in water were studied using static and dynamic light scattering techniques (SLS and DLS). All samples were equilibrated for at least for 1 day before measurements to ensure the stability of the aggregates. The parameters of the polymer micelles formed by the PEG-*b*-PADMO copolymers are summarized in Table 2. The  $M_{w,\text{app}}$  values of the micelles were in the range  $10^5$ – $10^6\ \text{g mol}^{-1}$  and increased with increasing PADMO block length. The  $M_{w,\text{app}}$  values for the micelles were 2 orders of magnitude larger than for the corresponding single-polymer chains (in THF), thus the polymers in the micelles had a large aggregation number  $N_{\text{agg}}$ . The hydrodynamic radius distributions of the polymer aggregates are shown in Figure S1 (Supporting Information). The hydrodynamic radius ( $R_h$ ) of the micelles varied in the range of 10–16 nm with narrow distributions and increased with increasing PADMO block length. However, the distribution was bimodal in the case of  $E_{45}A_{47}$  with the longest PADMO blocks. The bimodal distribution arose from the formation of larger ellipsoidal micelles, which was demonstrated directly via TEM images showing coexistence of small spherical micelles and larger wormlike micelles, as reported previously.<sup>27</sup> The high molecular weight  $M_{w,\text{app}}$  and



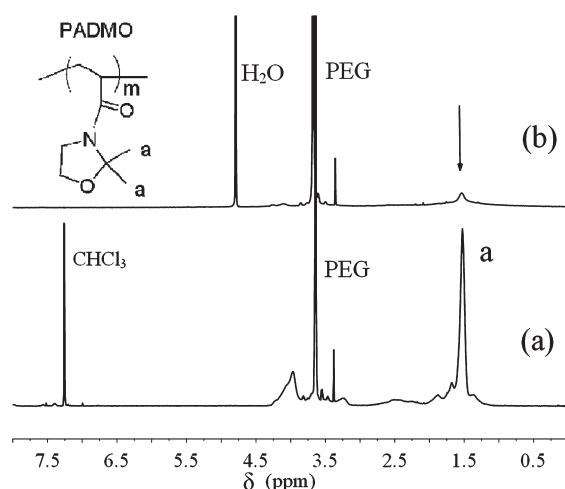
**Scheme 1. Chemical Structure of the PEG-*b*-PADMO Copolymer, Where *n* and *m* Represent the Degrees of Polymerization of the Respective Blocks**



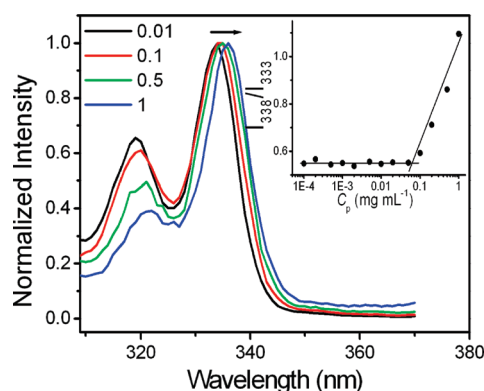
**Table 1. Molecular Weights, PDI, and CAC of the Copolymers**

sample	$M_w \times 10^{-3a}$ (g mol <sup>-1</sup> )	PDI <sup>a</sup> ( $M_w/M_n$ )	CAC <sup>b</sup> (mg mL <sup>-1</sup> )
E <sub>45</sub> A <sub>18</sub>	5.31	1.13	0.120
E <sub>45</sub> A <sub>28</sub>	6.46	1.14	0.065
E <sub>45</sub> A <sub>40</sub>	8.49	1.16	0.034
E <sub>45</sub> A <sub>47</sub>	9.19	1.13	0.029

<sup>a</sup> Determined by GPC (THF; polystyrene standards). <sup>b</sup> Determined by fluorescence spectroscopy using pyrene as a fluorescence probe.



**Figure 1.** <sup>1</sup>H NMR spectra of polymer E<sub>45</sub>A<sub>28</sub> dissolved in (a) CDCl<sub>3</sub> and (b) D<sub>2</sub>O.



**Figure 2.** Excitation spectra of pyrene in solutions of E<sub>45</sub>A<sub>28</sub> with different polymer concentration (mg mL<sup>-1</sup>). The inset shows the dependence of the intensity ratio ( $I_{338}/I_{333}$ ) of pyrene on polymer concentration.

large aggregation number  $N_{agg}$  together with the small size of the micelles demonstrate that the micelles formed from PEG-*b*-PADMO copolymers adopted a relatively compact structure in aqueous solution.

To further understand the details of the micellar structure, on the basis of the core-shell model and combination of DLS and SLS results, the core radius,  $R_{core}$ , shell thickness,  $R_{corona}$ , and density of PEG at the core-shell interface,  $\Phi_{PEG}$ , of the polymer micelles were evaluated and are listed in Table 2.  $R_h$  is the sum of the radius of the core ( $R_{core}$ ) and the shell thickness ( $R_{corona}$ ).  $R_{core}$  was calculated from the following equation<sup>28</sup>

$$R_{core} = \left( \frac{3M_{w,core}}{4\pi N_A \rho_{core}} \right)^{1/3} \quad (2)$$

where  $M_{w,core}$  is the weight average molecular weight of the core calculated from  $M_{w,app}$  values and the weight fractions of the PADMO block in the copolymers;  $N_A$  is Avogadro's number; and  $\rho_{core}$  is the density of the PADMO block, which was taken to be 1.05 g cm<sup>-3</sup> (the bulk density of ADMO monomer).<sup>28</sup> Thus, values of  $R_{core}$  and  $R_{corona}$  were calculated for the polymer micelles, as summarized in Table 2. It was found that the core radius  $R_{core}$  increased with increasing block length of the core-forming polymer in the order E<sub>45</sub>A<sub>18</sub> < E<sub>45</sub>A<sub>28</sub> < E<sub>45</sub>A<sub>40</sub> < E<sub>45</sub>A<sub>47</sub>, in parallel with the increase of the aggregation number. Theoretically, the length of a fully extended PEG chain with DP = 45 is 16 nm.<sup>31</sup> The thickness of the coronas of E<sub>45</sub>A<sub>18</sub>, E<sub>45</sub>A<sub>28</sub>, E<sub>45</sub>A<sub>40</sub>, and E<sub>45</sub>A<sub>47</sub> is less than half that value, suggesting that the PEG chains in the micelles did not have a fully elongated conformation. That is probably due to the fact that strong n-clustering attractive interactions caused collapse of the PEG chains, though the PEG chains densely packed in the shell were crowded and forced to stretch to avoid overlapping. Consequently, the PEG chains arranged in the shell were not only stretched but also compressed.<sup>32–34</sup>

The PEG chain density at the core-shell interface ( $\Phi_{PEG}$ ) was determined using the equation  $\Phi_{PEG} = N_{agg}/(4\pi R_{core}^2)$ .<sup>28,35</sup> The values of  $\Phi_{PEG}$  are almost the same for the micelles of each polymer, although the sizes and  $N_{agg}$  values of the micelles are different. The calculated  $\Phi_{PEG}$  values are about 0.30 chains/nm<sup>2</sup>, which is about twice the values reported for conventional polymer micelles. For example, the complex micelles of PEG-*b*-P(Asp)/PEG-*b*-P(Lys)<sup>35</sup> and PEG-*b*-P(DEAEMA/CEA)<sup>28</sup> were found to have  $\Phi_{PEG}$  values of 0.14 and 0.15 chains/nm<sup>2</sup>, respectively. This circumstantial evidence suggests a more densely packed PEG structure in the micelles of PEG-*b*-PADMO than in conventional polymer micelles.

The results expatiated above are similar to that reported by Hu and Wu.<sup>36,37</sup> They grafted PEG chains onto a thermally sensitive PNIPAM spherical microgel to form a kind of polymer brush. The grafting density can be varied with shrinking of the microgel at temperature higher than 32 °C. They found an expected shrinking of grafted PEG layer at temperature higher than ~33 °C, which was attributed to the n-clustering attractive interaction, inducing collapse of the PEG brushes as the grafting density increased. Therefore, chain collapse and the nonfully hydrated state would facilitate hydrophobic interaction upon heating, thereby causing decrease of LCST.<sup>38</sup>

**3.2. Thermoresponsive Phase Transition.** The thermally induced phase transition behavior of the PEG-*b*-PADMO diblock copolymer in aqueous solution was determined by

**Table 2. Parameters of Copolymer Micelles in Aqueous Solution Obtained from Light Scattering Data**

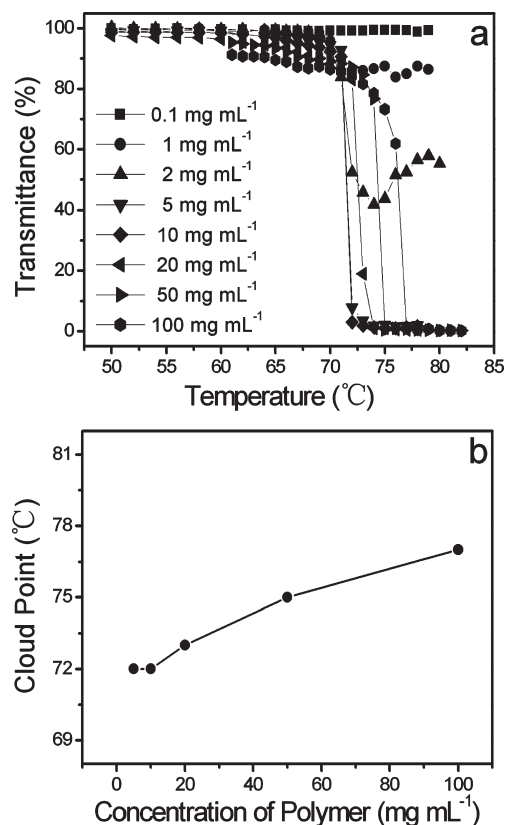
sample	$M_{w,app} \times 10^{-5a}$ (g mol <sup>-1</sup> )	$N_{agg}^b$	$R_h^c$ (nm)	$R_{core}$ (nm)	$R_{corona}$ (nm)	$\Phi_{PEG}$ (chains/nm <sup>2</sup> )
E <sub>45</sub> A <sub>18</sub>	4.69	88	10.0	4.61	5.39	0.33
E <sub>45</sub> A <sub>28</sub>	8.05	125	11.1	5.85	5.15	0.29
E <sub>45</sub> A <sub>40</sub>	25.6	301	13.0	8.91	4.09	0.30
E <sub>45</sub> A <sub>47</sub>	32.3	351	16.0 (93%) 90.0 (7%)	9.76	6.24	0.29

<sup>a</sup> Determined by static light scattering (SLS),  $C_p = 0.8$ – $5.0$  mg mL<sup>-1</sup>, 25 °C. <sup>b</sup> Calculated from the ratio of  $M_w$  values for the micelles and unimers obtained from SLS and GPC measurements, respectively. <sup>c</sup> Determined by dynamic light scattering (DLS),  $C_p = 1.0$  mg mL<sup>-1</sup>, 25 °C. 16.0 (93%) means 93 mass % of aggregates with hydrodynamic radius of 16.0 nm.

transmittance measurement; the macroscopic phase transition temperature was identified as the cloud point. The diblock copolymers consisted of hydrophobic PADMO and hydrophilic PEG blocks, wherein PADMO was acid-labile and nonthermosensitive. PEG is widely utilized as a water-soluble building block for many functional copolymer systems. PEG is also known to possess hydrophilic and hydrophobic dual character and undergo the LCST phase transition upon heating, in general above the boiling point of water. The PEG with molecular weight  $2.0 \times 10^3$  g mol<sup>-1</sup> (DP = 45) that was used as the hydrophilic block of the copolymers studied has LCST 170–180 °C.<sup>8–10</sup> Such PEG blocks in a copolymer should remain in a hydrophilic state and not undergo a LCST transition at temperatures below 100 °C. Unexpectedly, the thermal phase transition was found to occur in the copolymer micellar solutions within the broad tunable temperature range 40–72 °C, depending on the copolymer composition and structure that did not exist in the individual PEG precursor under the same conditions. Such a large change of PEG thermosensitivity may be attributed to the densely packed structure of PEG in the self-assemblies of the PEG-*b*-PADMO copolymers in water. The strong *n*-clustering attractive interaction induces collapse of PEG chains and forces water out because the PEG chain density in the shell of the micelles is as high as  $\sim 0.30$  chains/nm<sup>2</sup>. The resulting insufficient hydration structure would favor increasing the thermosensitivity and lowering the LCST via a cooperative process in phase transition.

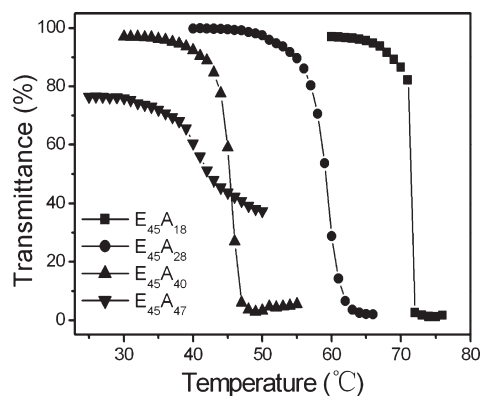
Similar results about densely packed structure effect on thermoresponsive ability have been reported by several groups.<sup>17,39–41</sup> For example, Zhu and Napper<sup>41</sup> observed that the PNIPAM chains anchored onto a surface have two types of coil-to-globule transitions due to the difference in polymer density between the inner and outer regions. Tenhu<sup>17</sup> and other groups<sup>39,40</sup> grafted PNIPAM onto the surface of particles and ascribed the double phase transition to the differences in polymer density and hydration between the inner and outer region of PNIPAM brushes, which was further explained by the *n*-clusters concept developed by de Gennes.<sup>42</sup> To the best of our knowledge, this phenomenon has been rarely observed for either individual PEG macromolecules or conventional thermoresponsive copolymers in dilute aqueous solution.<sup>43–48</sup> For those reasons, the thermal behavior of PEG-*b*-PADMO copolymer and the factors influencing the behavior were investigated in detail.

**Concentration Dependence.** Figure 3 shows the temperature dependence of the optical transmittance of E<sub>45</sub>A<sub>18</sub> aqueous solution as a function of concentration. For the lowest concentration (0.1 mg mL<sup>-1</sup>, which was below the CAC), nearly 100% transmittance was maintained in the tested temperature range. As the polymer concentration became higher than the CAC and



**Figure 3.** (a) Dependence of the LCST transition on the polymer concentration of E<sub>45</sub>A<sub>18</sub>. (b) Cloud point as a function of the concentration of E<sub>45</sub>A<sub>18</sub>.

micelle formation occurred, the transmittance decreased sharply at about 72 °C on heating, indicating that a LCST transition readily occurred only in micellar solution. The polymer concentration had a small effect on the LCST of the micellar solution: increasing the concentration from 1 to 100 mg mL<sup>-1</sup> shifted the cloud point 5 °C toward higher temperature. Similar observations have been reported for other thermosensitive polymers.<sup>26</sup> In addition, it should be noted that the sharpness of the thermally induced phase transition was dependent on the polymer concentration. A fairly sharp LCST transition at 72 °C was observed at concentrations of 5 and 10 mg mL<sup>-1</sup>. At concentrations of 1 and 2 mg mL<sup>-1</sup>, very limited variation of transmittance was displayed at the cloud point. For concentrations >10 mg mL<sup>-1</sup>, the transition became broader. Thus, a suitable concentration that provided a sufficient amount of the micelle aggregate particles without kinetically restricted aggregation during the



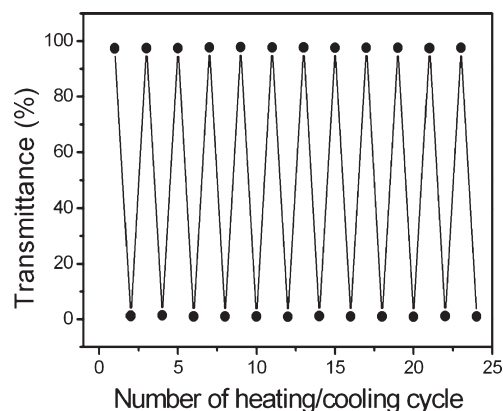
**Figure 4.** Effect of temperature on the transmittance of the micellar solutions of the four copolymers during heating.  $C_p = 5 \text{ mg mL}^{-1}$ .

thermally induced phase transition was necessary for precise LCST measurement.

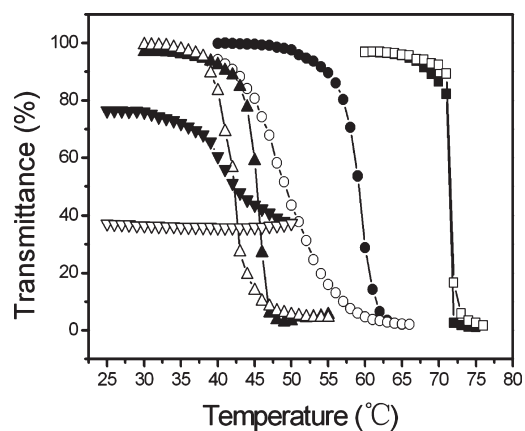
**Influence of Hydrophobic Block Length.** The hydrophilicity–hydrophobicity balance is the key factor for the phase transition of thermoresponsive polymers. The LCST transition behavior of the PEG-*b*-PADMO copolymers was easily tuned by changing the length of the hydrophobic PADMO block: the larger the hydrophobic block content of the copolymer, the lower the LCST at fixed PEG molecular weight. Figure 4 shows the temperature dependence of optical transmittance of micellar solutions of the four copolymers with different hydrophobic PADMO block lengths, at  $5 \text{ mg mL}^{-1}$  concentration (in each case above the CAC). The transmittance decreased significantly at a specific temperature on heating solutions of all of the copolymers except  $E_{45}A_{47}$ . The cloud point was evaluated as 72, 60, and 45 °C for  $E_{45}A_{18}$ ,  $E_{45}A_{28}$ , and  $E_{45}A_{40}$ , respectively, thus showing a decreasing trend with increasing PADMO block length.  $E_{45}A_{47}$  was less thermosensitive and underwent a relative smooth decrease in transmittance on heating, probably due to the coexistence of two kinds of micelles, namely, small spheres and large wormlike structures.

These results clearly show that the phase transition of PEG-*b*-PADMO can be controlled within a wide temperature range (40–72 °C) by varying the block length of the core-forming polymer. Similar observations have been reported for several thermosensitive polymers, but the extent of the variation in LCST with varying hydrophobicity was generally not very significant for those block copolymers. For example, the cloud point of the thermoresponsive polymer PEG-*b*-PNIPAM varied by only a few degrees when the DP of PEG block increased from 0 to 114.<sup>49</sup> The large difference between PEG-*b*-PADMO and common thermoresponsive block copolymers can be mainly attributed to the self-assembled structure of the micelle-forming copolymers and the dense structure of the PEG shell in the micelles.

**Reversible Behavior.** An interesting observation (Figure 5) is the excellent reversibility and reproducibility displayed by copolymer  $E_{45}A_{18}$  in the optical transmittance of the micellar solution during 12 cycles of temperature change between 50 °C (below the LCST) and 75 °C (above the LCST). The transparent micellar solution rapidly became cloudy when the temperature was increased from 50 to 75 °C and reverted to the transparent state when the solution was cooled from 75 to 50 °C. The highest and lowest transmittance of  $E_{45}A_{18}$  micellar solution remained almost constant during multiple heating–cooling cycles without



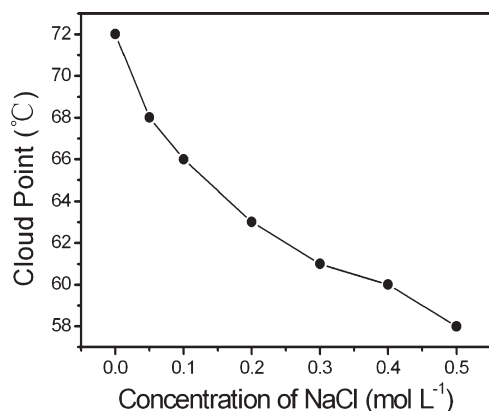
**Figure 5.** Reversible changes of optical transmittance in response to temperature fluctuations for  $E_{45}A_{18}$  micellar solution.  $C_p = 5 \text{ mg mL}^{-1}$ .



**Figure 6.** Transmittance versus temperature plots for various copolymer aqueous solutions ( $C_p = 5 \text{ mg mL}^{-1}$ ) during one heating–cooling cycle.  $E_{45}A_{18}$ : heating (■), cooling (□);  $E_{45}A_{28}$ : heating (●), cooling (○);  $E_{45}A_{40}$ : heating (▲), cooling (△);  $E_{45}A_{47}$ : heating (▼), cooling (▽).

any detectable hysteresis. This is due to lack of hydrogen bonding between these PEG-containing polymers in the assembled state, unlike that of PNIPAM. Consequently, they showed different behavior of thermally induced phase transition, compared to amide-containing polymer as reported previously.<sup>50–52</sup> However, hysteresis was observed for copolymers  $E_{45}A_{28}$  and  $E_{45}A_{40}$  with a greater proportion of hydrophobic PADMO, as shown in Figure 6. The most hydrophobic sample ( $E_{45}A_{47}$ ) showed nearly irreversible behavior under the same experimental conditions. We speculate that the hysteresis was due to the fact that greater hydrophobic character of the copolymer leads to formation of more stable, larger aggregates via intermicelle association, in which the larger hydrophobic domain and closely compact structure can prevent PEG rehydration by water upon cooling. Thus, the larger aggregates dissociated slowly to individual micelles. Similar results have been reported for some amphiphilic copolymers containing PEG hydrophilic segments.<sup>48,53–55</sup> It is believed that if the rate of cooling is sufficiently slow the hysteresis will disappear.<sup>50</sup>

**Salt Effect.** The phase transition behavior of thermoresponsive polymers in aqueous solution is known to be influenced by additives such as salts, surfactants, alcohols, etc. The reason is that these additives can alter the interactions between the



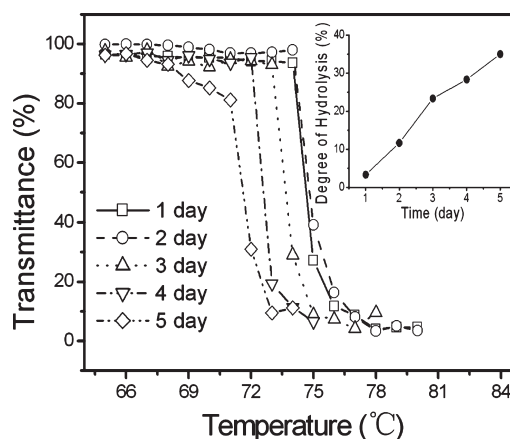
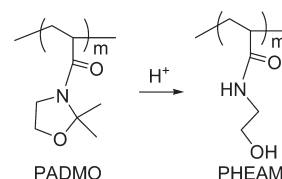
**Figure 7.** Effect of NaCl concentration on the cloud point of a micellar solution of  $E_{45}A_{18}$ .  $C_p = 5 \text{ mg mL}^{-1}$ .

polymer and water.<sup>56,57</sup> Sodium chloride (NaCl) as a typical water structure-maker (kosmotrope) can disrupt the hydration structure surrounding the polymer chains, leading to a salting-out effect and thereby lowering the cloud point of the polymer solution. Figure 7 displays the cloud point of  $E_{45}A_{18}$  micellar solution as a function of NaCl concentration: a typical salting-out effect was observed. The cloud point of the copolymer was found to decrease strongly with increasing salt concentration. It should be noted that the influence of added salt on thermal behavior was more marked for the PEG-*b*-PADMO copolymer than for the PNIPAM homopolymer. In this range of salt concentration ( $0\text{--}0.5 \text{ mol L}^{-1}$ ), the cloud point decreased more than  $10^\circ\text{C}$  for PEG-*b*-PADMO, whereas for PNIPAM the change in cloud point was reported to be just a few degrees.<sup>57</sup>

This observation can be explained by two different interaction mechanisms. According to the newer theories, the salt effect on PNIPAM solvation involves three factors related to the interaction of the ions with the polymer and its hydration waters: mainly polarization, surface tension, and specific ion binding.<sup>57–59</sup> The first and second factors should lead to salting-out of the polymer, thereby lowering the LCST. The salt ions disrupt hydrogen bonds and break up the ordered water structure surrounding the polymer, promoting hydrophobic polymer–polymer interaction, resulting from the polarization effect and increased surface tension. The third effect, anion binding directly to the amide groups of PNIPAM, should lead to salting-in of the polymer. However, the third effect is absent in the case of the PEG segments of the copolymer because the lone pair of electrons on the ether oxygen imparts anionic character to the polymer. Consequently, a combination of these influences obviously favors salting-out of polymer and lowering LCST for copolymer compared to PNIPAM. On the other hand, since the block copolymer in water forms micelles with a dense PEG shell, the added salt may influence the polymer micellar microstructure, including the PEG chain packing structure in the shell. As the density of the PEG structure increases, intensive *n*-clustering attractive interaction can induce greater collapse of PEG chains, leading to enhancement of thermosensitivity.

**Effect of Hydrolysis.** The PEG-*b*-PADMO copolymers contain pendant acid-labile oxazolidine side groups (ADMO) that undergo hydrolysis in acid media (see Scheme 2) to generate the hydrophilic product 2-hydroxyethyl acrylamide (HEAM),<sup>27</sup> resulting in increased hydrophilicity. Consequently, the phase transition of the copolymers should vary with the degree of

**Scheme 2.** Hydrolysis Process and Product of PADMO in an Acid Medium

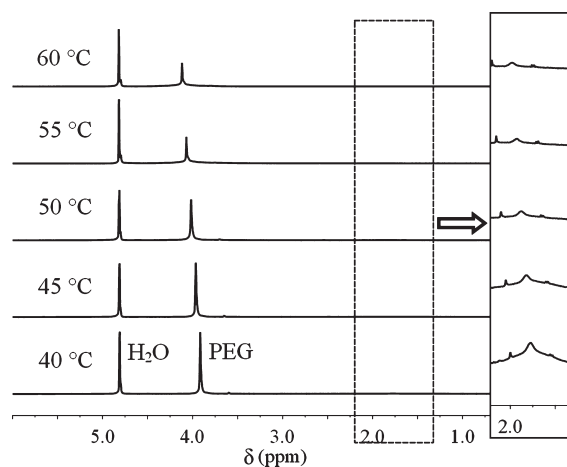


**Figure 8.** Transmittance versus temperature plots of solutions of  $E_{45}A_{18}$  for a range of hydrolysis times. The concentration of HCl was  $0.05 \text{ mol L}^{-1}$ . The inset shows the degree of hydrolysis as a function of time calculated from the  $^1\text{H}$  NMR spectra.  $C_p = 5 \text{ mg mL}^{-1}$ .

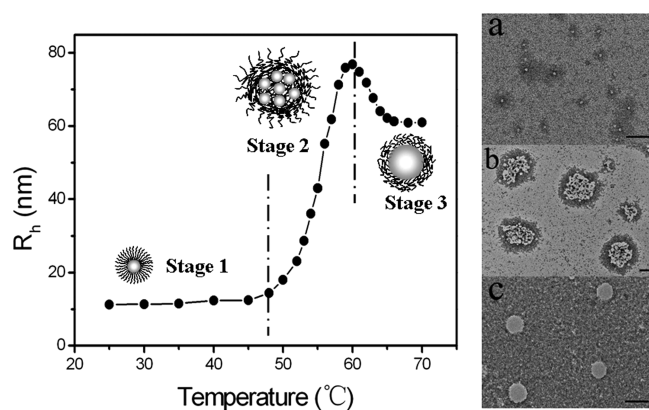
hydrolysis of the PADMO block. To verify this speculation, the LCST behavior of a micellar solution of  $E_{45}A_{18}$  that was pretreated by acid hydrolysis for various times at ambient temperature was determined by turbidimetry. To avoid destroying the micellar nanostructure, the study was limited to small degrees of hydrolysis. Figure 8 shows that the cloud point of the copolymer solution decreased gradually with increasing hydrolysis time. The corresponding variation of the degree of hydrolysis, calculated from  $^1\text{H}$  NMR spectra, is shown in the inset to Figure 8. This phenomenon is probably due to hydrogen bonding between PEG chains and amide or hydroxyl moieties of the hydrolysis product PHEAM in the copolymer, making the micelles more compact and thus decreasing the cloud point. This may be useful as a route to developing temperature-responsive materials with tunable LCST, like the PEG-*b*-PADMO block copolymer with hydrolyzable functionality.

**3.3. Aggregation Mechanism.** To better understand the mechanism of the thermally induced phase transition or separation of these polymer micelle systems at the molecular level,  $^1\text{H}$  NMR spectra of copolymer  $E_{45}A_{28}$  in  $\text{D}_2\text{O}$  were determined as a function of temperature; the spectra are shown in Figure 9. The water peak was used as an internal reference. The spectra are typical for a core–shell nanostructure, where the proton signals ( $3.8\text{--}4.0 \text{ ppm}$ ) of PEG were sharp and clear, indicating that the PEG corona of the micelle was in a well-solvated state. The signals ( $1.5\text{--}2.0 \text{ ppm}$ ) of the core-forming PADMO, on the other hand, were very weak because of its immiscibility and restricted motion. Upon increasing the temperature, the intensity of the PEG peak started to decrease, and the decrease became





**Figure 9.** Temperature-dependent  $^1\text{H}$  NMR spectra of  $\text{E}_{45}\text{A}_{28}$  in  $\text{D}_2\text{O}$  ( $10 \text{ mg mL}^{-1}$ ). The inset magnifies the spectra in the range 1.3–2.2 ppm.



**Figure 10.** Evolution of the hydrodynamic radius of the micelles of  $\text{E}_{45}\text{A}_{28}$  in the heating process and TEM images of the micelles at different temperatures. (a) 25 °C; (b) 60 °C; and (c) 65 °C. The scale bars are 100 nm.  $C_p = 0.5 \text{ mg mL}^{-1}$ .

significant at 50–60 °C, due to dehydration of PEG and induced chain collapse. By contrast, only a slight decrease in intensity was observed for the PADMO peaks (inset to Figure 9) during heating, confirming that there was almost no effect on the inner core as the temperature rose. These results support the hypothesis that thermally induced dehydration of PEG chains is the main driving force for the phase transition of the micellar solution. This becomes important for the dense chain packing in the PEG corona of the polymer micelles, where strong  $n$ -clustering interaction induces PEG chain collapse and reduces hydration, thus causing the LCST transition to take place at lower temperature. Figure 9 also shows that the peak intensity changed smoothly, with no evidence of new bond formation as the temperature was increased from 40 to 60 °C. This might reflect the fact that there was no substantial structural change in the micelle during the phase transition, and the core–shell structure was preserved. The NMR spectra are consistent with TEM images (Figure 10) which show that larger aggregates with multicore structure were present.

For further insight into the nature of the thermally induced aggregation of copolymer in aqueous solution, the morphology

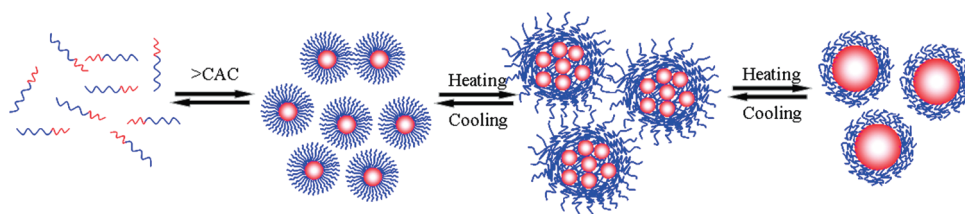
and structure transformation of polymeric aggregates during the LCST phase transition were studied by a combination of DLS and TEM measurements at different temperatures, below and above the LCST. Figure 10 shows the temperature dependence of the hydrodynamic radius ( $R_h$ ) of copolymer  $\text{E}_{45}\text{A}_{28}$  in solution. The dynamic plots can be divided into three temperature regions. When the solution temperature was below the LCST (<50 °C, Stage 1), spherical polymer micelles existed individually; there was almost no obvious change in size as temperature increased; and the micellar solution was clear. At temperatures close to the LCST (Stage 2), intermicelle aggregation gave rise to formation of larger aggregates with multicore structure that was detectable in their TEM images (Figure 10, inset b) and associated with an abrupt increase in aggregate radius to about 75 nm. Moreover, the solution became cloudy. This behavior is mostly due to the partial dehydration of PEG altering the hydrophilic–hydrophobic balance of the micelles and inducing the micelle aggregates to restore the balance.<sup>48</sup> Interestingly, it was found that as the temperature further increased beyond 60 °C (Stage 3) the larger polymeric aggregates became unstable and that the particle size diminished with temperature, then approached a plateau. This was the result of formation of relatively large globular bilayer aggregates with average radius 60 nm, via fusion driven by further dehydration of PEG and thermal chain motion. Note that if the copolymer concentration is higher than  $5 \text{ mg mL}^{-1}$  macrophase separation will occur, and coacervate droplet formation and precipitation will be observed in the third stage.

By combining the  $^1\text{H}$  NMR analysis and TEM observation of morphology changes, we can draw a conclusion regarding the mechanism of the thermally induced phase transition of PEG-*b*-PADMO in water; the proposed mechanism is depicted in Scheme 3. Primarily, the amphiphilic diblock copolymers self-assembled into well-defined core–shell type micelles with high aggregation number in water. The densely packed PEG shell structure in micelles played a significant role in determination of their thermal behavior, being similar to that of highly dense PNIPAM brushes bound to the surface of nanoparticles.<sup>17</sup> The densely packed PEG shell structure resulted in insufficient hydration and greatly enhanced the thermosensitivity.<sup>60</sup> As a consequence, when the polymer micellar solution was heated to the LCST, partial dehydration of the PEG corona caused by partial breaking of ether–water hydrogen bonds decreased the hydrophilicity of the PEG corona. Thus, the polymer micelles aggregated into larger aggregates with multicore structure by increasing hydrophobic interaction and intermicelle overlapping. In this case, however, dehydration of the PEG shell was not sufficiently strong to completely destroy the core–shell micellar structure. However, as the temperature was further increased beyond the LCST, the larger aggregates, essentially aggregated multimicelles, further fused with each other and reorganized into bigger vesicle-like nanostructures together with a small amount of rodlike micelles (Figure S2, Supporting Information). This structure forms a stable suspension which remains cloudy if the concentration is relatively low. However, if the concentration is high, the micelles would further coagulate and precipitate.

Clearly, this type of micelle-forming thermosensitive copolymer differs markedly from conventional thermosensitive polymers in terms of its specific self-assembly and structure with high density, which plays a crucial role in determining the thermosensitive properties.



Scheme 3. Schematic Illustration of Thermally Induced Aggregation and Phase Transition of Copolymers in Water



#### 4. CONCLUSIONS

We developed a convenient route to thermoresponsive block copolymers based on linear PEG as a hydrophilic block and with temperature-sensitive functionality, whose thermal behavior can be controlled by the self-assembled structure over a wide temperature range. The amphiphilic PEG-*b*-PADMO diblock copolymer, a thermoresponsive polymer of this type, formed well-defined core-shell micelles, having hydrophobic PADMO core and hydrophilic PEG corona, with high aggregation number in water. The densely packed PEG shell structure in the polymer micelles resulted in insufficient hydration via  $\pi$ -clustering attractive interaction at lower temperatures and substantial enhancement of thermosensitivity. Thus, the thermal phase transition of the polymer solutions, via intermicelle aggregation driven by dehydration of PEG on heating, occurs at moderate temperatures far lower than that of the PEG homopolymer precursor, which is commonly above the boiling point of water. The cloud points of these copolymers can be controlled in the temperature range 40–72 °C by varying the block length of PADMO at fixed PEG content, whereas the cloud point of the PEG precursor with similar molecular weight ( $2.0 \times 10^3 \text{ g mol}^{-1}$ ) was in the range 170–180 °C. The cloud points of the copolymers can also be modulated by partial hydrolysis of the PADMO segments. The unique properties and characteristics of this type of thermosensitive copolymer are expected to be utilized for exploring novel functional materials, which are not obtainable with conventional thermosensitive polymers.

#### ■ ASSOCIATED CONTENT

**Supporting Information.** DLS results of the copolymers and TEM image of the micelles of  $E_{45}A_{28}$  above LCST. This material is available free of charge via the Internet at <http://pubs.acs.org>.

#### ■ AUTHOR INFORMATION

##### Corresponding Author

\*Tel.: +86 10 82543569. Fax: +86 10 82543491. E-mail: [fpwu@mail.ipc.ac.cn](mailto:fpwu@mail.ipc.ac.cn).

#### ■ REFERENCES

- (1) Mano, J. F. *Adv. Eng. Mater.* **2008**, *10*, 515–527.
- (2) He, C. L.; Kim, S. W.; Lee, D. S. *J. Controlled Release* **2008**, *127*, 189–207.
- (3) Wu, C.; Wang, X. H. *Phys. Rev. Lett.* **1998**, *80*, 4092–4094.
- (4) Xia, Y.; Burke, N. A. D.; Stöver, H. D. H. *Macromolecules* **2006**, *39*, 2275–2283.
- (5) Bianco-Peled, H.; Gryc, S. *Langmuir* **2004**, *20*, 169–174.
- (6) Wu, J. Y.; Liu, S. Q.; Heng, P. W. S.; Yang, Y. Y. *J. Controlled Release* **2005**, *102*, 361–372.

- (7) Duncan, R. *Nat. Rev. Drug Discovery* **2003**, *2*, 347–360.
- (8) Saeki, S.; Kuwahara, N.; Nakata, M.; Kaneko, M. *Polymer* **1976**, *17*, 685–689.
- (9) Bae, Y. C.; Lambert, S. M.; Soane, D. S.; Prausnitz, J. M. *Macromolecules* **1991**, *24*, 4403–4407.
- (10) Ashbaugh, H. S.; Paulaitis, M. E. *Ind. Eng. Chem. Res.* **2006**, *45*, 5531–5537.
- (11) Lutz, J.-F.; Akdemir, Ö.; Hoth, A. *J. Am. Chem. Soc.* **2006**, *128*, 13046–13047.
- (12) Lutz, J.-F.; Hoth, A. *Macromolecules* **2006**, *39*, 893–896.
- (13) Luzon, M.; Boyer, C.; Peinado, C.; Corrales, T.; Whittaker, M.; Tao, L.; Davis, T. P. *J. Polym. Sci., Part A: Polym. Chem.* **2010**, *48*, 2783–2792.
- (14) Han, S.; Hagiwara, M.; Ishizone, T. *Macromolecules* **2003**, *36*, 8312–8319.
- (15) Ishizone, T.; Seki, A.; Hagiwara, M.; Han, S. *Macromolecules* **2008**, *41*, 2963–2967.
- (16) Hua, F. J.; Jiang, X. G.; Zhao, B. *Macromolecules* **2006**, *39*, 3476–3479.
- (17) Shan, J.; Chen, J.; Nuopponen, M.; Tenhu, H. *Langmuir* **2004**, *20*, 4671–4676.
- (18) Rezende, C. A.; Shan, J.; Lee, L. T.; Zalczer, G.; Tenhu, H. *J. Phys. Chem. B* **2009**, *113*, 9786–9794.
- (19) Haba, Y.; Harada, A.; Takagishi, T.; Kono, K. *J. Am. Chem. Soc.* **2004**, *126*, 12760–12761.
- (20) Haba, Y.; Kojima, C.; Harada, A.; Kono, K. *Macromolecules* **2006**, *39*, 7451–7453.
- (21) Haba, Y.; Kojima, C.; Harada, A.; Kono, K. *Angew. Chem., Int. Ed.* **2007**, *46*, 234–237.
- (22) Kojima, C.; Yoshimura, K.; Harada, A.; Sakanishi, Y.; Kono, K. *Bioconjugate Chem.* **2009**, *20*, 1054–1057.
- (23) Carter, S.; Hunt, B.; Rimmer, S. *Macromolecules* **2005**, *38*, 4595–4603.
- (24) Cheng, H. X.; Yuan, X. J.; Sun, X. Y.; Li, K. P.; Zhou, Y. F.; Yan, D. Y. *Macromolecules* **2010**, *43*, 1143–1147.
- (25) Liu, H. J.; Chen, Y.; Shen, Z. *J. Polym. Sci., Part A: Polym. Chem.* **2007**, *45*, 1177–1184.
- (26) Zhou, Y. F.; Yan, D. Y.; Dong, W. Y.; Tian, Y. *J. Phys. Chem. B* **2007**, *111*, 1262–1270.
- (27) Cui, Q. L.; Wu, F. P.; Wang, E. J. *Polymer* **2011**, *52*, 1755–1765.
- (28) Yusa, S.; Sugahara, M.; Endo, T.; Morishima, Y. *Langmuir* **2009**, *25*, 5258–5265.
- (29) Bae, J. W.; Lee, E.; Park, K. M.; Park, K. D. *Macromolecules* **2009**, *42*, 3437–3442.
- (30) Bougard, F.; Giacomelli, C.; Mespouille, L.; Borsali, R.; Dubois, Ph.; Lazzaroni, R. *Langmuir* **2008**, *24*, 8272–8279.
- (31) Tanford, C.; Nozakli, Y.; Rohde, M. F. *J. Phys. Chem.* **1977**, *81*, 1555–1560.
- (32) Chen, H. W.; Zhang, Q. J.; Li, J. F.; Ding, Y. W.; Zhang, G. Z.; Wu, C. *Macromolecules* **2005**, *38*, 8045–8050.
- (33) Petrov, P.; Rangelov, S.; Novakov, C.; Brown, W.; Berlinova, I.; Tsvetanov, C. B. *Polymer* **2002**, *43*, 6641–6651.
- (34) Nagarajan, R.; Ganesh, K. *J. Colloid Interface Sci.* **1996**, *184*, 489–499.
- (35) Harada, A.; Kataoka, K. *Macromolecules* **2003**, *36*, 4995–5001.

- (36) Hu, T. J.; Wu, C. *Macromolecules* **2001**, *34*, 6802–6805.
- (37) Hu, T. J.; Wu, C. *Phys. Rev. Lett.* **1999**, *83*, 4105–4107.
- (38) Li, W.; Zhang, A. F.; Feldman, K.; Walde, P.; Schlüter, A. D. *Macromolecules* **2008**, *41*, 3659–3667.
- (39) Wu, T.; Zhang, Y. F.; Wang, X. F.; Liu, S. Y. *Chem. Mater.* **2008**, *20*, 101–109.
- (40) Tsuji, S.; Kawaguchi, H. *Macromolecules* **2006**, *39*, 4338–4344.
- (41) Zhu, P. W.; Napper, D. H. *Colloids Surf., A* **1996**, *113*, 145–153.
- (42) Wagner, M.; Brochard-Wyart, F.; Hervet, H.; de Gennes, P.-G. *Colloid Polym. Sci.* **1993**, *271*, 621–628.
- (43) Dimitrov, I.; Trzebicka, B.; Müller, A. H. E.; Dworak, A.; Tsvetanov, C. B. *Prog. Polym. Sci.* **2007**, *32*, 1275–1343.
- (44) Wei, H.; Cheng, S. X.; Zhang, X. Z.; Zhuo, R. X. *Prog. Polym. Sci.* **2009**, *34*, 893–910.
- (45) Choi, B. G.; Sohn, Y. S.; Jeong, B. J. *Phys. Chem. B* **2007**, *111*, 7715–7718.
- (46) Yan, J. J.; Ji, W. X.; Chen, E. Q.; Li, Z. C.; Liang, D. H. *Macromolecules* **2008**, *41*, 4908–4913.
- (47) Virtanen, J.; Tenhu, H. *Macromolecules* **2000**, *33*, 5970–5975.
- (48) Jeong, B.; Windisch, C. F., Jr.; Park, M. J.; Sohn, Y. S.; Gutowska, A.; Char, K. J. *Phys. Chem. B* **2003**, *107*, 10032–10039.
- (49) Zhu, K. Z.; Pamies, R.; Kjøniksen, A. L.; Nyström, B. *Langmuir* **2008**, *24*, 14227–14233.
- (50) Berber, M. R.; Mori, H.; Hafez, I. H.; Minagawa, K.; Tanaka, M.; Niidome, T.; Katayama, Y.; Maruyama, A.; Hirano, T.; Maeda, Y.; Mori, T. J. *Phys. Chem. B* **2010**, *114*, 7784–7790.
- (51) Ding, Y. W.; Ye, X. D.; Zhang, G. Z. *Macromolecules* **2005**, *38*, 904–908.
- (52) Cheng, H.; Shen, L.; Wu, C. *Macromolecules* **2006**, *39*, 2325–2329.
- (53) Liang, X. F.; Guo, C.; Ma, J. H.; Wang, J.; Chen, S.; Liu, H. Z. *J. Phys. Chem. B* **2007**, *111*, 13217–13220.
- (54) Qiao, Z. Y.; Du, F. S.; Zhang, R.; Liang, D. H.; Li, Z. C. *Macromolecules* **2010**, *43*, 6485–6494.
- (55) Kim, S. Y.; Kim, H. J.; Lee, K. E.; Han, S. S.; Sohn, Y. S.; Jeong, B. *Macromolecules* **2007**, *40*, 5519–5525.
- (56) Durme, K. V.; Rahier, H.; Mele, B. V. *Macromolecules* **2005**, *38*, 10155–10163.
- (57) Zhang, Y. J.; Furry, S.; Bergbreiter, D. E.; Cremer, P. S. *J. Am. Chem. Soc.* **2005**, *127*, 14505–14510.
- (58) Boström, M.; Williams, D. R. M.; Ninham, B. W. *Biophys. J.* **2003**, *85*, 686–694.
- (59) Boström, M.; Williams, D. R. M.; Ninham, B. W. *Phys. Rev. Lett.* **2001**, *87*, 16803.
- (60) Elliott, I. G.; Kuhl, T. L.; Faller, R. *Macromolecules* **2010**, *43*, 9131–9138.